Macromolecules

pubs.acs.org/Macromolecules Article

# Nanoconfinement and Salt Synergistically Suppress Crystallization in Polyethylene Oxide

Zheng Zhang, Junjun Ding, Benjamin M. Ocko, Julien Lhermitte, Joseph Strzalka, Chang-Hwan Choi, Frank T. Fisher, Kevin G. Yager,* and Charles T. Black*

Cite This: https://dx.doi.org/10.1021/acs.macromol.9b01725 Read Online

ACCESS | Metrics & More | Article Recommendations | Supporting Information

**ABSTRACT:** Suppressing the crystallization of polyether-based solid electrolytes is a widely sought-after strategy to improve ionic conductivity. We report the effects of nanoconfinement on polyethylene oxide electrolytes. We find that neat polyethylene oxide responds to nanoconfinement by adopting a preferred orientation yet is able to crystallize even in nanoconfinement volumes with widths as small as 8 nm. However, the combination of nanoconfinement and salt addition does suppress polymer crystallization at room temperature even though either factor alone cannot. Such synergistic suppression of crystallization has implications for polymer electrolytes since amorphous rather than crystalline domains predominantly contribute to ionic conduction. Our results suggest that salts previously discounted due to their inability to suppress crystallinity in bulk materials could be made viable when combined with nanoconfinement, thereby opening new possibilities for high-performance solid polymer electrolytes.

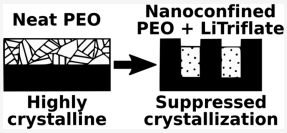


## ■ INTRODUCTION

Polyethers, most notably polyethylene oxide (PEO), find use in a broad range of applications, including as solid polymer electrolytes (SPE) in lithium-ion batteries.[1] Compared with the traditional organic-solvent-based liquid electrolytes, SPEs are safer because they are less flammable and more resistant to mechanical impact.[2] In order for PEO to function as an ionic conductor, it must be blended with a lithium salt, such as lithium bis(trifluoromethanesulfonyl) imide (LiTFSI) or lithium trifluoromethanesulfonate (LiTriflate). Under a directional electric field, dissociated lithium ions move within the amorphous domains of PEO, facilitated by segmental relaxation of flexible molecular chains.[3,4] In contrast, the rigid crystalline domains block ionic transport and thus hinder conductivity.[1] The high degree of crystallinity typical for PEO at room temperature gives rise to an ionic conductivity that is 3 orders of magnitude lower than typical liquid electrolytes.[5] Suppression of PEO crystallization has long been sought as a way to bring the transport performance of PEO closer to that of liquid electrolytes.[6] Confinement of PEO has been proposed as a means of controlling polymer crystallization and has thus been studied in a variety of contexts,[1,7,8] including in thin films,[9−11] in droplets,[12] in nanocomposites[13] and blends,[14−16] in the nanopores of aluminum oxide templates,[17−20] within one of the domains of a self-assembling block copolymer morphology,[5,6,21−24] and using other nanomaterials.[25−28] These studies established that confinement can alter chain configurations and dynamics,[17,26,27,29] crystal orientation,[18,30] and crystallization kinetics.[9,25] Moreover, confinement can suppress crystallization under appropriate conditions.[6,26,31] Mixing PEO with certain salts can also inhibit crystallization because the association between salt ions and crown ethers acts as dynamic "cross-links", disrupting orderly chain packing, while the dissociated anions plasticize the polymer. This effect is notable for LiTFSI, which strongly suppresses PEO crystallization, and thereby enables ion conductivity even at room temperature.[32] However, many other salts do not readily suppress crystallization or may even form a cocrystal with the polymer, prohibiting free migration of ions. Thus, a number of polymer and salt combinations are presumptively excluded from applications.

In this work, we explore a new strategy for controlling polymer crystallization using nanoconfinement of hybrid polymer/ionic materials. We demonstrate that crystallization of certain PEO/lithium salt mixtures can be suppressed via nanoconfinement, even in cases when the salt cocrystallizes with PEO in the bulk. Our results suggest a synergistic phenomenon where only the combination of both nanoconfinement and salt addition can efficiently disrupt the strong crystallization of PEO.

## ■ RESULTS AND DISCUSSION

PEO readily crystallizes at room temperature; for instance, low-molecular-weight PEO can easily reach a bulk crystallinity of 98%.[33] Crystallization is a significant hindrance to using PEO-based electrolytes in commercial batteries due to the extremely limited lithium-ion conductivity of crystalline polymer domains. To quantify the crystallinity and crystal orientation of PEO in films, we employ grazing-incidence wide-angle X-ray scattering (GIWAXS). GIWAXS measure-

Received: August 16, 2019
Revised: November 23, 2019

ments on a thick PEO film (~1 μm) ($M_w$ = 430 kg/mol, denoted as PEO430*k*) yield a scattering image with bright and sharp rings, indicative of high crystallinity without preferred molecular orientation (Figure S1). Our measurements on films as thin as 50 nm demonstrate that PEO remains highly crystalline even when considerably confined in the film-thickness direction (Figure 1a).

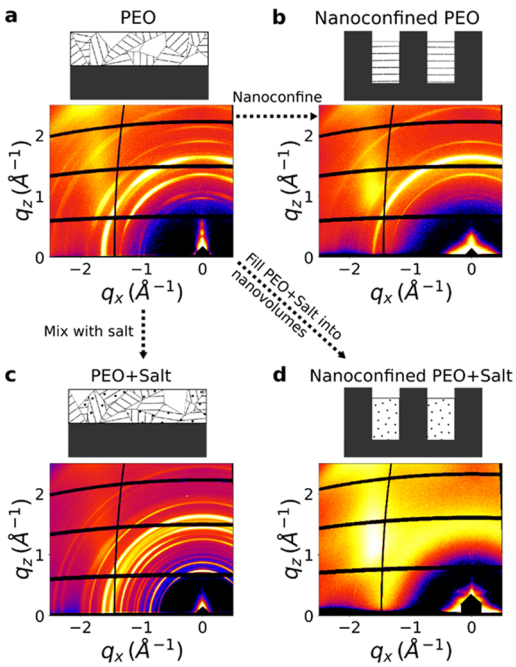


**Figure 1.** Sample schematic and GIWAXS images of (a) PEO430*k* thin film (~50 nm), (b) PEO430*k* confined in ~110 nm wide nanogratings, (c) PEO/LiTriflate thin film (~200 nm), and (d) PEO/LiTriflate mixture confined in ~110 nm wide nanogratings. GIWAXS images are shown as the ($q_x$, $q_z$) projection, with the $q_y$ component omitted in plotting but retained for subsequent calculations.

Nanoscale confinement is a powerful strategy for controlling molecular organization, with previous studies reporting that confinement of certain polymers into nanovolumes with size comparable to the chain size scale can frustrate molecular packing and may disrupt crystallization.[34−38] However, confinement has not been previously shown to suppress PEO crystallization. In this work, we probe PEO under different size scales of two-dimensional (2D) confinement—including distances as small as 8 nm—and find that the neat polymer crystallizes even in strongly confined geometries. We fabricated nanoscale line grating grooves in silicon as confining environments using high-resolution laser interference lithography[39,40] and dry plasma etching.[41] We systematically varied the scale of the confinement by using atomic layer deposition to coat the grating walls and progressively shrink the groove volume (Figure S2). These nanogratings were filled with PEO by spin-coating from acetonitrile followed by vacuum annealing at 85 °C (higher than the melting temperature of PEO, ~65 °C) for 1 h. The solution concentration and spin-coating speed were optimized to fill the grating grooves without overfilling (Figures S2 and S3). GIWAXS patterns of PEO confined within nanogratings (example shown in Figure 1b) show strong and anisotropic scattering rings, indicating a high degree of crystallinity—comparable to that seen in a thin film of similar volume (Figure 1a). The scattering patterns are anisotropic, indicating preferential orientation of the PEO crystal grains with respect to the grating sidewalls. Previous studies of PEO confined in anodized alumina nanopores (3D confinement) similarly observed reorientation of PEO crystals.[18] We observe strong crystallinity across 2D confinement size scales of 8, 35, and 110 nm, demonstrating that even extreme nanoconfinement does not significantly suppress PEO crystallization.

The scattering pattern of a thin film of the same PEO, unconfined but instead loaded with LiTriflate salt, contains two sets of peaks: the peaks observed for neat crystalline PEO and a set of peaks that can be ascribed to a PEO/LiTriflate salt complex (cocrystal) (Figure 1c). In this sample, the salt concentration (23% by weight) yields a ratio of 0.085:1 between the $Li^+$ ions and the PEO repeat-units. The coexistence of pure PEO crystalline domains and crystalline complex domains is consistent with previous reports of the phase diagram for this system[32,42] and shows that LiTriflate salt does not inhibit PEO crystallization but instead leads to the formation of coexisting crystalline domains.

In contrast to nanoconfined neat PEO, GIWAXS images of the nanoconfined PEO/LiTriflate mixture do not exhibit any sharp peaks (Figure 1d), indicating that crystallization of both PEO and the salt complex have been entirely suppressed. The PEO/LiTriflate mixture was filled into nanofabricated gratings in a similar manner to the pure polymer since both PEO and LiTriflate are miscible in acetonitrile. The observed suppressed crystallization of the nanoconfined mixture is especially remarkable because neither confinement nor salt mixing is able to prevent PEO crystallization on its own. The two effects combine synergistically, suppressing both PEO and salt crystallization and transforming the mixture into a homogeneous single phase (amorphous solid solution of PEO and salt).

To explore the origin of this synergistic effect, we systematically studied the influence of confinement and salt addition on PEO crystallization. Neat PEO (without any salt) confined within grooves with 110 nm width remains highly crystalline, with the crystal domains becoming oriented by the confinement (Figure 1b). Systematically increasing the degree of confinement more strongly orients the polymer (Figure 2), indicating that PEO interacts strongly with the groove walls across the size range studied here (110 to 8 nm). Figure 2 shows X-ray scattering results for three different molecular weights of PEO (430*k*, 39*k*, and 4*k*) confined within three different groove widths. The amorphous $AlO_x$ used to coat the gratings (and thereby shrink the confinement volume) contributes to the diffuse scattering, especially in the narrowest gratings; nevertheless, the scattering of PEO remains sufficiently strong that it can be resolved above this background. Nanoconfinement does not alter the PEO lattice constant, even in the smallest grating widths (Figure S5). Background-subtracted angular cuts of intensities taken along an arc at constant $q$ = 1.362 Å$^{-1}$ (the (120) PEO reflection) quantify the PEO orientation distribution under different degrees of nanoconfinement (Figure 2b−d). All molecular weight/grating width combinations show a monomodal orientation distribution, suggesting a single preferred alignment direction for PEO confined to nanogratings.

We observe a narrower orientation distribution for samples that are more strongly confined, confirming that the PEO crystallites are orienting strongly in response to the confine-


https://dx.doi.org/10.1021/acs.macromol.9b01725
Macromolecules XXXX, XXX, XXX−XXX

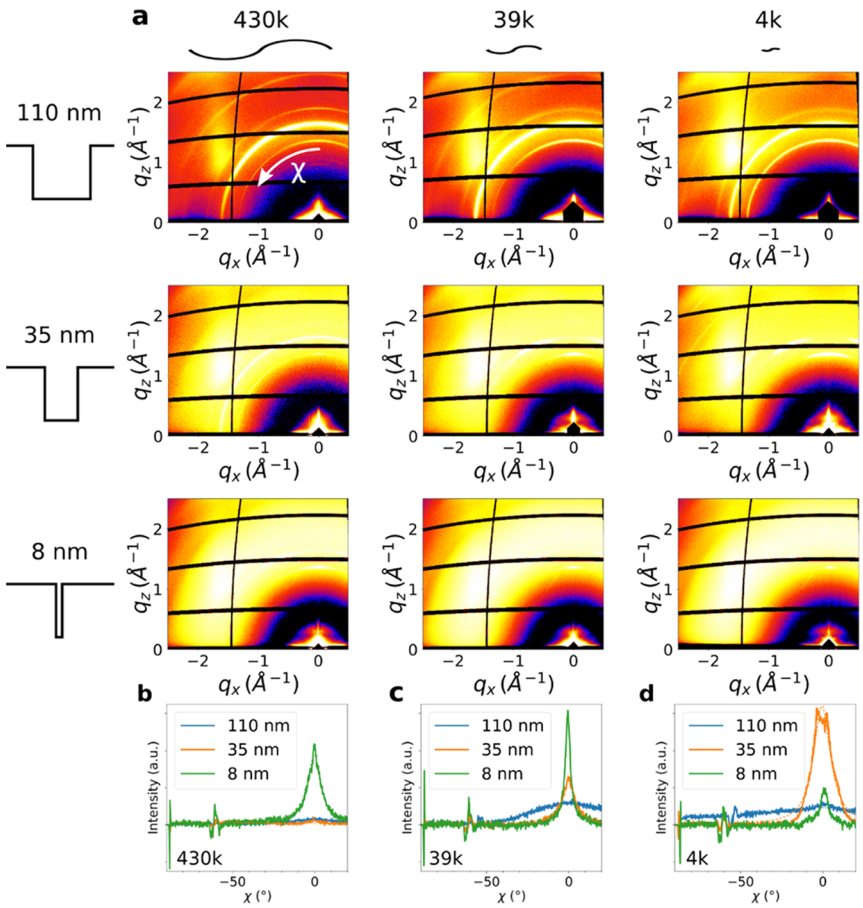


**Figure 2.** (a) GIWAXS images of PEO ($M_w$ = 430, 39, and 4 kg/mol) confined in nanogratings of groove widths (100, 35, and 8 nm). Background-subtracted angular cuts of scattering intensities along an arc at constant $q$ = 1.362 Å$^{-1}$ are shown below, highlighting the orientation distribution of the (120) peak, for (b) $M_w$ = 430 kg/mol, (c) $M_w$ = 39 kg/mol, and (d) $M_w$ = 4 kg/mol. Dashed lines are Lorentzian fits.

ment interfaces. We extract the full width at half-maximum (FWHM) of the angular cuts by fitting them to a Lorentzian function. Smaller confinement size scales induce stronger orientation of PEO (smaller FWHM, Figure 3). This systematic trend is observed when reducing groove width for a fixed PEO molecular weight and similarly when increasing PEO molecular weight in confined within a fixed groove width (Figure 3), confirming that PEO chain packing is responsive to the nanoconfinement environment. Interestingly, PEO packs into well-defined crystalline domains even in the most extreme confinement of 8 nm grating width, a dimension comparable with the critical PEO nucleus size (1−10 nm).[19] The robust crystallization of PEO at such an ultrasmall size scale[12] can be compared to other polymers such as polypropylene where crystallization was suppressed under more modest confinement (∼20 nm).[38] The difference in size scale required for suppression of crystallization for different polymers may arise due to differences in polymer chain properties, which in turn affect the critical nucleation size scale. Flexible polymers (PEO has a persistence length of 3.8 Å)[43−45] will be able to rearrange even under confinement to nucleate crystal domains, while for more rigid polymers (polypropylene has a persistence length of >5 Å),[46] motion will be arrested.

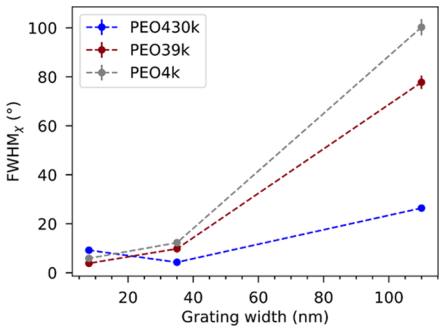


**Figure 3.** Full width at half-maximum (FWHM) of the angular distribution of the PEO (120) peak as a function of nanograting width, for different molecular weights: (blue) $M_w$ = 430 kg/mol, (brown) $M_w$ = 39 kg/mol, and (gray) $M_w$ = 4 kg/mol. Error bars denote the uncertainty of Lorentzian peak fits. Similar trends are observed for angular spread of other PEO crystalline peaks.

We next consider the influence of combined confinement and mixing with lithium salt on PEO crystallization. Crystalline domains of PEO produce two signature peaks at $q$ = 1.362 Å$^{-1}$ and $q$ = 1.653 Å$^{-1}$, indicated by the vertical dashed lines in the 1D intensity $I(q)$ versus $q$ plots (Figure 4a and Figure S4). The former is indexed to the (120) plane, and the latter represents a collection of planes: 112/032/$\bar{1}$32/$\bar{2}$12 (Figure S7 and Table S1), in agreement with previous structural analysis.[47] The thin-film measurement provides a baseline for understanding the effects of nanoconfinement as well as salt mixing. Nano-confined PEO shows these same two peaks (Figure 4b); however, the 1.362 Å$^{-1}$ peak has reduced intensity, which can be attributed to the PEO preferential orientation. Addition of LiTriflate salt (0.085 concentration, in terms of the $Li^+$/EO


https://dx.doi.org/10.1021/acs.macromol.9b01725
Macromolecules XXXX, XXX, XXX−XXX

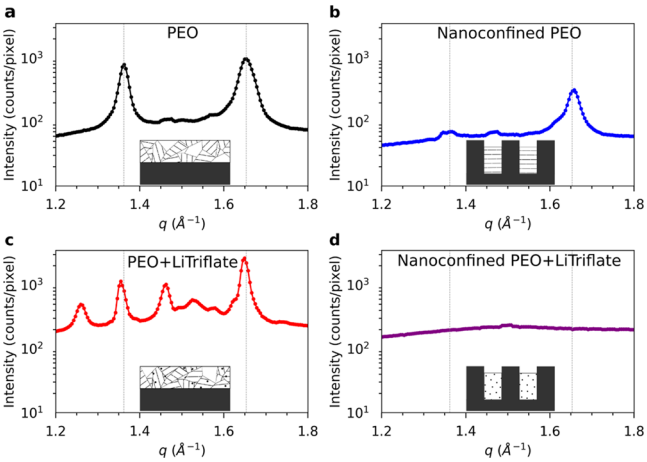


**Figure 4.** 1D scattering intensity $I(q)$ as a function of $q$ for (a) a PEO430$k$ film, (b) PEO430$k$ confined in ∼110 nm wide nanogratings, (c) a PEO430$k$/LiTriflate mixture film, and (d) PEO430$k$/LiTriflate mixture confined in ∼110 nm nanogratings. $I(q)$ is calculated by integrating and averaging over $\chi$ for each given $q$. Measurements were conducted ∼2 weeks after sample preparation.

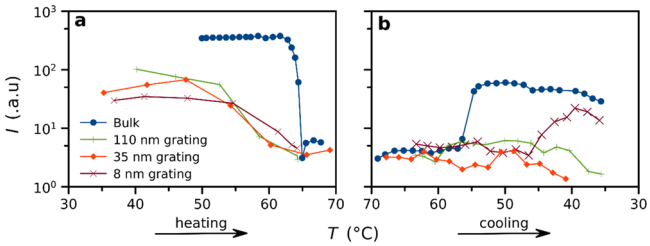


**Figure 5.** Integrated peak intensity at $q$ = 1.362 Å$^{-1}$ measured in situ during (a) heating and (b) cooling (1 °C/min ramp) for PEO430$k$ in bulk (blue circles) and confined to nanogratings of widths: 110 (green crosses), 35 (red diamonds), and 8 nm (brown multiplication symbols).

ratio[48]) does not inhibit crystallization (Figure 4c), but a mixture of the same concentration of LiTFSI renders the PEO completely amorphous (Figure S6c). In the PEO/LiTriflate mixture, the PEO peaks are slightly shifted to lower $q$, consistent with a slight expansion of the crystalline unit cell. The additional scattering peaks seen in the mixture (Figure 4c and Figure S8) arise from the stoichiometric $PEO_3$:LiTriflate cocrystal.[49] The coexistence of PEO and $PEO_3$:LiTriflate crystals for this mixing ratio is consistent with previous reports.[32]

Even though neither nanoconfinement (Figure 4b) nor mixing with LiTriflate salt (Figure 4c) alone can suppress PEO crystallization, the combined effect of both of these is to strongly suppress PEO crystallization and thus render the PEO amorphous (Figure 4d). This synergistic effect inhibits both crystalline PEO and $PEO_3$:LiTriflate domain formation, as is clear by comparing Figure 4c,d. The confinement size scale (110 nm) can be compared to the polymer radius of gyration (∼40 nm).[50] Suppression of crystallization may be due to thermodynamic effects, kinetic effects, or a combination. For instance, nanoconfinement could raise the energy of crystalline domains relative to amorphous or shift the crystallization temperature. Confinement may also inhibit polymer mobility, thereby kinetically trapping the material in a supersaturated amorphous state.

We conducted in situ thermal annealing experiments to probe the melting and crystallization behavior of neat PEO under confinement. These data indicate that both melting and crystallization of neat PEO are slower under nanoconfinement than those of bulk materials (Figure 5)—suggesting that while nanoconfinement cannot completely suppress crystallization, it strongly frustrates the ability of the polymer to rearrange into crystalline domains. Thick films (∼1 $\mu$m) of PEO430$k$ and the same PEO confined to nanogratings were first slowly heated (1 °C/min) to 70 °C and then cooled to room temperature at the same rate. Figure 5 shows the integrated peak intensity ($q$ = 1.362 Å$^{-1}$) as a function of temperature during the thermal cycling. The bulk PEO (blue circles) melts at $T_m \approx 63$ °C and crystallizes when supercooled to ∼10 °C below $T_m$, which agrees well with literature data on bulk PEO.[46] The nanograting-confined PEO exhibited an earlier onset of melting (∼53 °C) and a broad melt transition for all confining groove widths. This is consistent with previous studies of PEO confined to anodized alumina nanopores and has been interpreted as the result of thinner lamella formed under confinement (the thickness of lamellae crystals inversely correlates with $T_m$, according to the Gibbs−Thomson equation).[18,19] Most importantly, the slope of the intensity decay in Figure 5a shows that the nanoconfined samples melt significantly slower than the corresponding bulk sample, suggesting a slowdown in the unpacking of confined polymer chains.

Upon cooling (Figure 5b), we similarly observe a delay and slower kinetics for crystallization of the nanoconfined material than that for the bulk. The nanoconfined PEO crystallizes much more slowly—in some cases not achieving measurable crystallinity within the experimental window (Figure 5b). However, we confirmed that pure nanoconfined PEO does eventually crystallize (starting point of curves in Figure 5a; see also Figure S9). This frustrated crystallization under confinement evidently proceeds over a timescale of days at room temperature. The overall crystallization rate has underlying contributions from at least two kinetic phenomena: the rate of nucleation ($K_n$) and the rate of crystal growth ($K_g$). Since $K_g$ is related to the kinetics of polymer chains attaching/detaching from an existing crystal surface, this term is expected to be reduced for confined crystallization, similar to confined melting, owing to the hindering of polymer motion over the large length scales required for the cooperative rearrangement associated with crystallization. Indeed, studies on PEO thin films (<100 nm) measured a growth rate $K_g$ lower than that in the bulk material or thick films.[9,51] The overall influence of nanoconfinement on $K_n$ is more complicated and involves competing size effects and surface effects. Because nanoconfinement reduces the population of impurities (potential nuclei) within each confined volume, $K_n$ is expected to decrease when heterogeneous nucleation is suppressed in favor of the more difficult homogeneous nucleation (size effect).[19,52] The confining sidewalls themselves could conceivably act as nucleation sites, promoting heterogeneous nucleation (surface effect) and counteracting the size effect. We do observe more rapid crystallization at the smallest confinement scale (8 nm, Figure 5b), which can be rationalized in terms of a stronger surface effect for 8 nm confinement compared to 35 and 110 nm nanogratings. However, previous reports indicate that confinement walls do not induce heterogeneous nucleation.[20] This suggests that elimination of the bulk heterogeneous


https://dx.doi.org/10.1021/acs.macromol.9b01725
Macromolecules XXXX, XXX, XXX−XXX

nucleation pathway explains the observed delayed crystallization under confinement.

Overall, the influence of nanoconfinement on PEO melting and crystallization rates suggests that the observed synergistic suppression of crystallization—when combining confinement and salt—is fundamentally kinetic (Figure 4d). It is well known that solvated lithium salts raise the glass transition temperature $T_g$,[53] therefore reducing chain mobility and correspondingly slowing the growth factor $K_g$. The formation of the salt-rich $PEO_3$:LiTriflate nuclei and salt-depleted PEO nuclei relies on the transport of salt ions, which is hindered due to the bulkiness of the anions, thus also reducing $K_n$. Thus, both nanoconfinement and salt complexation will slow the overall kinetics of polymer crystallizations, with both the nucleation rate and crystal growth rate being reduced. When combined, the kinetic hindrances of confinement and salt addition combine multiplicatively, leading to a greatly reduced rate for crystallization. In particular, we observe that the rate of crystallization for PEO/LiTriflate is hindered to the point that it does not crystallize over practical timescales (Figure S10 shows no detectable crystallization after 16 months at room temperature).

## ■ CONCLUSIONS

We report the influence of nanoconfinement, a mixture with lithium salts, and combinations of these two factors on the crystallization behavior of PEO. Neat PEO crystallized within nanoconfining grooves exhibits a preferred orientation, templated by the grating sidewalls, with alignment becoming stronger as the confinement size scale is reduced. However, our results indicate that 2D nanoconfinement alone is insufficient to suppress PEO crystallization, even when the size scale of confinement is as small as 8 nm. Combining nanoconfinement and addition of the lithium salt LiTriflate synergistically suppresses PEO crystallization even though neither confinement alone nor addition of LiTriflate alone prevents crystal formation. These fundamental results suggest that nanoconfinement could be considered as a possible strategy for creating materials with tailored functional properties. For instance, this strategy could have use in high-performance solid electrolytes for room-temperature ion conducting applications (such as batteries) since the suppression of crystal formation greatly enhances PEO ionic transport. The observed synergistic effect moreover opens the door toward using salts that were previously discounted because they could not suppress PEO crystallinity, and thus mixtures of these exhibit poor room-temperature conductivity. The present results suggest that new classes of PEO/salt mixtures could be considered for electrolyte applications if combined with nanoconfining geometries.

## ■ METHODS

**Materials.** Monodispersed dihydroxy-terminated polyethylene oxide (PEO) of molecular weights ($M_w$) 4, 39, and 430 kg/mol was used as received from Polymer Source, Inc. Bis(trifluoromethane) sulfonimide lithium salt (LiTFSI), lithium trifluoromethanesulfonate (LiTriflate), and acetonitrile (anhydrous, 99.8%) were obtained from Sigma-Aldrich, Inc.

**Fabrication.** We used n-type crystalline Si(100) wafers (0.001−0.005 Ω·cm) for fabricating the nanostructured templates. A thin layer of MCC Primer 80/20 (MicroChem), spin-coated at 7000 rpm, was used as an adhesion promoter. NR7-250P (Futurrex, Inc.), spin-coated at 7000 rpm for 40 s, was used as the (negative) resist layer and baked on a hot plate at 150 °C for 1 min prior to exposure to yield a resist thickness of ∼150 nm. A custom 2 degrees of freedom Lloyd-mirror Interferometer built with a 325 nm wavelength HeCd laser (model IK3501R-G, Kimmon Koha Co., Ltd.) was used for exposure.[39] The exposure was performed to a total dose of 7 mJ/cm$^2$, at an exposure angle (between the sample surface normal and the laser beam) of 53°, yielding a periodicity of 270 nm. The post-exposure samples were baked at 100 °C for 1 min, developed in RD6 (Futurrex, Inc., diluted to 33.3 vol % with deionized water) for 6 s, rinsed in deionized water for 30 s, and finally dried with a nitrogen gun.

Reactive ion etching (Oxford Instruments Plasmalab 100) was used to transfer the resist pattern into the Si substrate via an automated two-step etching recipe: (1) 40 sccm $SF_6$, 18 sccm $O_2$, 15 mtorr, −100 °C, ICP 800 W, RF 40 W for 3 s; (2) 7 W for 60 s. We used *n*-methyl-2-pyrrolidone (NMP) to strip the remaining resist. The above procedure yielded nanogratings with trenches 110 nm wide. To vary the size scale of confinement, the trench width was reduced to 35 and 8 nm (Figure S2) by coating the sidewalls with $AlO_x$ using atomic layer deposition.

Prior to filling the nanopatterned substrates with PEO, substrates were cleaned with $O_2$ plasma on a March etcher (100 mtorr, RF 20 W for 3 min). Polymer materials were spin-coated from an acetonitrile solution onto the substrates in a humidity-controlled dry room followed by vacuum baking at 85 °C (above the melting transition of bulk PEO, ca 65 °C and well above its glass transition temperature) for 1 h to remove the residual solvent and help PEO filling the nanovolumes.[54] The concentration of the solution and spinning speed were controlled for optimum filling (no over filling), which was confirmed using SEM imaging of neat polymer samples as well as samples infiltrated with an inorganic material to improve imaging conditions. Salt-mixed PEO was weighed to a controlled $Li^+$:EO ratio of 0.085 (23% by weight for LiTriflate, 36% by weight for LiTFSI), dissolved in acetontrile, and filled into the nanovolumes using the same approach. Samples were stored in sealed, argon-filled, polypropylene-lined vacuum pouches before X-ray measurements.

**Characterization.** The thicknesses of spin-coated PEO films were measured with a Filmetrics reflectometer. We used a Hitachi S-4800 scanning electron microscope (SEM) to examine the total amount of filled material by imaging the edge of cleaved samples. To help cleave PEO, which is ductile under ambient conditions, we converted the PEO into a brittle inorganic composite using sequential infiltration synthesis to load the polymer with $AlO_x$.[55]

Grazing-incidence wide-angle X-ray scattering (GIWAXS) measurements were performed at 8-ID-E beamline of the Advanced Photon Source, Argonne National Laboratory, with a fixed photon energy of 10.86 keV (photon wavelength $\lambda$ = 1.142 Å). Samples were mounted on a thermal stage under vacuum. Data was collected across a range of incident angles (both below and above the film−vacuum critical angle). Data presented in the manuscript was acquired at 0.4°, which probes the entire film depth and limits the in-plane projected size of the beam. Acquired detector data were corrected for detector pixel-to-pixel sensitivity variations (flat-field) before further analysis. Conversion to $q$-space was calibrated using measurements of a reference sample (silver behenate) and knowledge of the beamline configuration. Detector images are converted into reciprocal-space before analysis; scattering images shown in the main text are displayed as the ($q_x$, $q_z$) projection, where $q_z$ is the vertical direction (film normal), $q_x$ is in the film plane and orthogonal the X-ray beam, and $q_y$ is along the beam direction. Thus, the smaller $q_y$ component is ignored for plotting purposes but is used internally for other calculations, including computing the total scattering $q$. For the in situ annealing experiments, the beam was periodically realigned due to thermal expansion. Only data taken immediately after realignment were used for this study.

For the angular cuts of scattering intensities, we define the angle $\chi$ such that $\chi = 0°$ corresponds to the vertical direction ($q_z$ axis) and $\chi = \pm 90°$ corresponds to the horizontal direction ($q_x$). This angle is defined with respect to the ($q_x$, $q_z$) projection; that is, we define $\chi$ to be the angle with respect to the $q_z$ axis within the ($q_x$, $q_z$) plane (as opposed to the smallest angle between the $q_z$ axis and the given point


https://dx.doi.org/10.1021/acs.macromol.9b01725
Macromolecules XXXX, XXX, XXX−XXX

on the surface of the curved Ewald sphere). Data remapping to $q$-space implicitly handles the intensity correction factors associated with the solid angle subtended by detector pixels. No polarization correction was applied to the data. When extracting the scattering intensity across $\chi$ at $q$ = 1.362 Å$^{-1}$, the background introduced by $AlO_x$ is removed by subtracting the arithmetic mean of two neighboring angular cuts: one at slightly lower $q$ = 1.257 Å$^{-1}$ and another slightly higher $q$ = 1.476 Å$^{-1}$. The background subtraction brings the baseline of all angular cuts down to 0, which confirms the correctness of the method used. For the 1D circular average scattering intensity $I(q)$, we sum the data at a given $q$ over the entire available range of angles $\chi$, excluding areas such as intermodule gaps that have been masked and normalizing by the number of pixels included in the sum (the angle range is roughly from $\chi = -90°$ to $\chi = 0°$).

Follow-up GIWAXS experiments, after holding samples at room temperature for 16 months, were performed at the Complex Materials Scattering (CMS, 11-BM) beamline of the National Synchrotron Light Source II (NSLS-II) at a fixed photon energy of 13.5 keV ($\lambda$ = 0.9184 Å).

## ■ ASSOCIATED CONTENT

### Supporting Information

The Supporting Information is available free of charge at https://pubs.acs.org/doi/10.1021/acs.macromol.9b01725.

SEM images showing filling of PEO into nanogrooves, GIWAXS data showing analysis methods, crystalline peaks across a wide range of $q$, peak position/width as a function of grating pitch, GIWAXS images showing the order of samples after extended aging at room temperature (PDF)

## ■ AUTHOR INFORMATION


### Corresponding Authors

**Kevin G. Yager** − *Center for Functional Nanomaterials, Brookhaven National Laboratory, Upton, New York 11973, United States*; orcid.org/0000-0001-7745-2513; Email: kyager@bnl.gov

**Charles T. Black** − *Center for Functional Nanomaterials, Brookhaven National Laboratory, Upton, New York 11973, United States*; Email: ctblack@bnl.gov

### Authors

**Zheng Zhang** − *Center for Functional Nanomaterials, Brookhaven National Laboratory, Upton, New York 11973, United States*

**Junjun Ding** − *Department of Mechanical Engineering, Stevens Institute of Technology, Hoboken, New Jersey 07030, United States*; orcid.org/0000-0002-7025-0617

**Benjamin M. Ocko** − *National Synchrotron Light Source II, Brookhaven National Laboratory, Upton, New York 11973, United States*; orcid.org/0000-0003-2596-1206

**Julien Lhermitte** − *National Synchrotron Light Source II, Brookhaven National Laboratory, Upton, New York 11973, United States*

**Joseph Strzalka** − *X-ray Science Division, Argonne National Laboratory, Argonne, Illinois 60439, United States*; orcid.org/0000-0003-4619-8932

**Chang-Hwan Choi** − *Department of Mechanical Engineering, Stevens Institute of Technology, Hoboken, New Jersey 07030, United States*; orcid.org/0000-0003-2715-7393

**Frank T. Fisher** − *Department of Mechanical Engineering, Stevens Institute of Technology, Hoboken, New Jersey 07030, United States*

Complete contact information is available at: https://pubs.acs.org/10.1021/acs.macromol.9b01725


### Author Contributions

Z.Z., B.M.O., K.G.Y., and C.T.B. designed the experiments. J.D. performed laser interference lithography exposure and development under the supervision of C.-H.C. and F.T.F. Z.Z. completed the bulk of nanofabrication and sample preparation. Z.Z., B.M.O., K.G.Y., and J.L. performed GIWAXS measurements with assistance from J.S. Z.Z. performed numerical analysis and prepared figures with feedback from B.M.O., K.G.Y., and C.T.B. Z.Z., K.G.Y., and C.T.B. wrote the manuscript. All authors reviewed and contributed to the manuscript.

### Notes

The authors declare no competing financial interest.

## ■ ACKNOWLEDGMENTS

This research was carried out at the Center for Functional Nanomaterials and the National Synchrotron Light Source II, which are U.S. DOE Office of Science Facilities, at Brookhaven National Laboratory under Contract No. DE-SC0012704. Research also used resources of the Advanced Photon Source, operated by Argonne National Laboratory under Contract No. DE-AC02-06CH11357. This work was partially supported by the Laboratory Directed Research and Development Program (LDRD) at Brookhaven National Laboratory.

## ■ REFERENCES


(1) Hallinan, D. T., Jr.; Balsara, N. P. Polymer Electrolytes. *Annu. Rev. Mater. Res.* **2013**, *43*, 503−525.

(2) Xue, Z.; He, D.; Xie, X. Poly(ethylene oxide)-based electrolytes for lithium-ion batteries. *J. Mater. Chem. A* **2015**, *3*, 19218−19253.

(3) Agapov, A. L.; Sokolov, A. P. Decoupling Ionic Conductivity from Structural Relaxation: A Way to Solid Polymer Electrolytes? *Macromolecules* **2011**, *44*, 4410−4414.

(4) Wang, Y.; Agapov, A. L.; Fan, F.; Hong, K.; Yu, X.; Mays, J.; Sokolov, A. P. Decoupling of Ionic Transport from Segmental Relaxation in Polymer Electrolytes. *Phys. Rev. Lett.* **2012**, *108*, No. 088303.

(5) Singh, M.; Odusanya, O.; Wilmes, G. M.; Eitouni, H. B.; Gomez, E. D.; Patel, A. J.; Chen, V. L.; Park, M. J.; Fragouli, P.; Iatrou, H.; Hadjichristidis, N.; Cookson, D.; Balsara, N. P. Effect of Molecular Weight on the Mechanical and Electrical Properties of Block Copolymer Electrolytes. *Macromolecules* **2007**, *40*, 4578−4585.

(6) Suzuki, Y.; Duran, H.; Steinhart, M.; Butt, H.-J.; Floudas, G. Suppression of Poly(ethylene oxide) Crystallization in Diblock Copolymers of Poly(ethylene oxide)-b-poly($\varepsilon$-caprolactone) Confined to Nanoporous Alumina. *Macromolecules* **2014**, *47*, 1793−1800.

(7) Colmenero, J.; Arbe, A. Segmental dynamics in miscible polymer blends: recent results and open questions. *Soft Matter* **2007**, *3*, 1474−1485.

(8) Lin, M.-C.; Nandan, B.; Chen, H.-L. Mediating polymer crystal orientation using nanotemplates from block copolymer microdomains and anodic aluminium oxide nanochannels. *Soft Matter* **2012**, *8*, 7306−7322.

(9) Dalnoki-Veress, K.; Forrest, J. A.; Massa, M. V.; Pratt, A.; Williams, A. Crystal growth rate in ultrathin films of poly(ethylene oxide). *J. Polym. Sci., Part B: Polym. Phys.* **2001**, *39*, 2615−2621.

(10) Hsiao, M.-S.; Chen, W. Y.; Zheng, J. X.; Van Horn, R. M.; Quirk, R. P.; Ivanov, D. A.; Thomas, E. L.; Lotz, B.; Cheng, S. Z. D. Poly(ethylene oxide) Crystallization within a One-Dimensional Defect-Free Confinement on the Nanoscale. *Macromolecules* **2008**, *41*, 4794−4801.

(11) Cheng, S.; Smith, D. M.; Li, C. Y. Anisotropic Ion Transport in a Poly(ethylene oxide)−$LiClO_4$ Solid State Electrolyte Templated by Graphene Oxide. *Macromolecules* **2015**, *48*, 4503−4510.

(12) Massa, M. V.; Carvalho, J. L.; Dalnoki-Veress, K. Confinement Effects in Polymer Crystal Nucleation from the Bulk to Few-Chain Systems. *Phys. Rev. Lett.* **2006**, *97*, 247802.

(13) Ahn, J. H.; Wang, G. X.; Liu, H. K.; Dou, S. X. Nanoparticle-dispersed PEO polymer electrolytes for Li batteries. *J. Power Sources* **2003**, *119-121*, 422−426.

(14) He, Z.; Liang, Y.; Han, C. C. Confined Nucleation and Growth of Poly(ethylene oxide) on the Different Crystalline Morphology of Poly(butylene succinate) From a Miscible Blend. *Macromolecules* **2013**, *46*, 8264−8274.

(15) Chen, N.; Yan, L.-T.; Xie, X.-M. Interplay between Crystallization and Phase Separation in PS-b-PMMA/PEO Blends: The Effect of Confinement. *Macromolecules* **2013**, *46*, 3544−3553.

(16) Samanta, P.; Thangapandian, V.; Singh, S.; Srivastava, R.; Nandan, B.; Liu, C.-L.; Chen, H.-L. Crystallization behaviour of poly(ethylene oxide) under confinement in the electrospun nanofibers of polystyrene/poly(ethylene oxide) blends. *Soft Matter* **2016**, *12*, 5110−5120.

(17) Lagrené, K.; Zanotti, J.-M. Anodic aluminium oxide: Concurrent SEM and SANS characterisation. Influence of AAO confinement on PEO mean-square displacement. *Eur. Phys. J.: Spec. Top.* **2007**, *141*, 261−265.

(18) Guan, Y.; Liu, G.; Gao, P.; Li, L.; Ding, G.; Wang, D. Manipulating Crystal Orientation of Poly(ethylene oxide) by Nanopores. *ACS Macro Lett.* **2013**, *2*, 181−184.

(19) Suzuki, Y.; Duran, H.; Steinhart, M.; Butt, H.-J.; Floudas, G. Homogeneous crystallization and local dynamics of poly(ethylene oxide) (PEO) confined to nanoporous alumina. *Soft Matter* **2013**, *9*, 2621−2628.

(20) Suzuki, Y.; Steinhart, M.; Kappl, M.; Butt, H.-J.; Floudas, G. Effects of polydispersity, additives, impurities and surfaces on the crystallization of poly(ethylene oxide)(PEO) confined to nanoporous alumina. *Polymer* **2016**, *99*, 273−280.

(21) Gomez, E. D.; Panday, A.; Feng, E. H.; Chen, V.; Stone, G. M.; Minor, A. M.; Kisielowski, C.; Downing, K. H.; Borodin, O.; Smith, G. D.; Balsara, N. P. Effect of Ion Distribution on Conductivity of Block Copolymer Electrolytes. *Nano Lett.* **2009**, *9*, 1212−1216.

(22) Majewski, P. W.; Gopinadhan, M.; Jang, W.-S.; Lutkenhaus, J. L.; Osuji, C. O. Anisotropic Ionic Conductivity in Block Copolymer Membranes by Magnetic Field Alignment. *J. Am. Chem. Soc.* **2010**, *132*, 17516−17522.

(23) Bouchet, R.; Maria, S.; Meziane, R.; Aboulaich, A.; Lienafa, L.; Bonnet, J.-P.; Phan, T. N. T.; Bertin, D.; Gigmes, D.; Devaux, D.; Denoyel, R.; Armand, M. Single-ion BAB triblock copolymers as highly efficient electrolytes for lithium-metal batteries. *Nat. Mater.* **2013**, *12*, 452.

(24) Chintapalli, M.; Le, T. N. P.; Venkatesan, N. R.; Mackay, N. G.; Rojas, A. A.; Thelen, J. L.; Chen, X. C.; Devaux, D.; Balsara, N. P. Structure and Ionic Conductivity of Polystyrene-block-poly(ethylene oxide) Electrolytes in the High Salt Concentration Limit. *Macromolecules* **2016**, *49*, 1770−1780.

(25) Wang, H.; Keum, J. K.; Hiltner, A.; Baer, E. Crystallization Kinetics of Poly(ethylene oxide) in Confined Nanolayers. *Macromolecules* **2010**, *43*, 3359−3364.

(26) Barroso-Bujans, F.; Fernandez-Alonso, F.; Cerveny, S.; Parker, S. F.; Alegría, A.; Colmenero, J. Polymers under extreme two-dimensional confinement: Poly(ethylene oxide) in graphite oxide. *Soft Matter* **2011**, *7*, 7173−7176.

(27) Barroso-Bujans, F.; Palomino, P.; Cerveny, S.; Fernandez-Alonso, F.; Rudić, S.; Alegría, A.; Colmenero, J.; Enciso, E. Confinement of poly(ethylene oxide) in the nanometer-scale pores of resins and carbon nanoparticles. *Soft Matter* **2013**, *9*, 10960−10965.

(28) Barroso-Bujans, F.; Cerveny, S.; Alegría, Á.; Colmenero, J. Chain Length Effects on the Dynamics of Poly(ethylene oxide) Confined in Graphite Oxide: A Broadband Dielectric Spectroscopy Study. *Macromolecules* **2013**, *46*, 7932−7939.

(29) Martín, J.; Krutyeva, M.; Monkenbusch, M.; Arbe, A.; Allgaier, J.; Radulescu, A.; Falus, P.; Maiz, J.; Mijangos, C.; Colmenero, J.; Richter, D. Direct Observation of Confined Single Chain Dynamics by Neutron Scattering. *Phys. Rev. Lett.* **2010**, *104*, 197801.

(30) Wang, H.; Keum, J. K.; Hiltner, A.; Baer, E. Impact of Nanoscale Confinement on Crystal Orientation of Poly(ethylene oxide). *Macromol. Rapid Commun.* **2010**, *31*, 356−361.

(31) Sinturel, C.; Vayer, M.; Erre, R.; Amenitsch, H. Nanostructured Polymers Obtained from Polyethylene-block-poly(ethylene oxide) Block Copolymer in Unsaturated Polyester. *Macromolecules* **2007**, *40*, 2532−2538.

(32) Vallée, A.; Besner, S.; Prud'Homme, J. Comparative study of poly(ethylene oxide) electrolytes made with LiN(CF3SO2)2, LiCF3SO3 and LiClO4: Thermal properties and conductivity behaviour. *Electrochim. Acta* **1992**, *37*, 1579−1583.

(33) Machado, J. C.; Silva, G. G.; Oliveira, F. C. d.; Lavall, R. L.; Rieumont, J.; Licinio, P.; Windmüller, D. Free-volume and crystallinity in low molecular weight poly(ethylene oxide). *J. Polym. Sci., Part B: Polym. Phys.* **2007**, *45*, 2400−2409.

(34) Shin, K.; Woo, E.; Jeong, Y. G.; Kim, C.; Huh, J.; Kim, K.-W. Crystalline Structures, Melting, and Crystallization of Linear Polyethylene in Cylindrical Nanopores. *Macromolecules* **2007**, *40*, 6617−6623.

(35) Wu, H.; Wang, W.; Yang, H.; Su, Z. Crystallization and Orientation of Syndiotactic Polystyrene in Nanorods. *Macromolecules* **2007**, *40*, 4244−4249.

(36) Wu, H.; Wang, W.; Huang, Y.; Wang, C.; Su, Z. Polymorphic Behavior of Syndiotactic Polystyrene Crystallized in Cylindrical Nanopores. *Macromolecules* **2008**, *41*, 7755−7758.

(37) Martín, J.; Mijangos, C.; Sanz, A.; Ezquerra, T. A.; Nogales, A. Segmental Dynamics of Semicrystalline Poly(vinylidene fluoride) Nanorods. *Macromolecules* **2009**, *42*, 5395−5401.

(38) Duran, H.; Steinhart, M.; Butt, H.-J.; Floudas, G. From Heterogeneous to Homogeneous Nucleation of Isotactic Poly(propylene) Confined to Nanoporous Alumina. *Nano Lett.* **2011**, *11*, 1671−1675.

(39) Wathuthanthri, I.; Mao, W.; Choi, C.-H. Two degrees-of-freedom Lloyd−mirror interferometer for superior pattern coverage area. *Opt. Lett.* **2011**, *36*, 1593−1595.

(40) Ding, J.; Du, K.; Wathuthanthri, I.; Choi, C.-H.; Fisher, F. T.; Yang, E.-H. Transfer patterning of large-area graphene nanomesh via holographic lithography and plasma etching. *J. Vac. Sci. Technol., B* **2014**, *32*, No. 06FF01.

(41) Johnston, D. E.; Lu, M.; Black, C. T. Plasma etch transfer of self-assembled polymer patterns. *J. Micro/Nanolithogr., MEMS, MOEMS* **2012**, *11*, No. 031306.

(42) Zardalidis, G.; Ioannou, E.; Pispas, S.; Floudas, G. Relating Structure, Viscoelasticity, and Local Mobility to Conductivity in PEO/LiTf Electrolytes. *Macromolecules* **2013**, *46*, 2705−2714.

(43) Mark, J. E.; Flory, P. J. The Configuration of the Polyoxyethylene Chain. *J. Am. Chem. Soc.* **1965**, *87*, 1415−1423.

(44) Kienberger, F.; Pastushenko, V. P.; Kada, G.; Gruber, H. J.; Riener, C.; Schindler, H.; Hinterdorfer, P. Static and Dynamical Properties of Single Poly(Ethylene Glycol) Molecules Investigated by Force Spectroscopy. *Single Mol.* **2000**, *1*, 123−128.

(45) Lee, H.; Venable, R. M.; MacKerell, A. D., Jr.; Pastor, R. W. Molecular Dynamics Studies of Polyethylene Oxide and Polyethylene Glycol: Hydrodynamic Radius and Shape Anisotropy. *Biophys. J.* **2008**, *95*, 1590−1599.

(46) Mark, J. E. *Polymer Data Handbook*; (2nd Edition). Oxford University Press: 2009.

(47) Takahashi, Y.; Tadokoro, H. Structural Studies of Polyethers, (−(CH2)m-O-)n. X. Crystal Structure of Poly(ethylene oxide). *Macromolecules* **1973**, *6*, 672−675.

(48) Teran, A. A.; Tang, M. H.; Mullin, S. A.; Balsara, N. P. Effect of molecular weight on conductivity of polymer electrolytes. *Solid State Ionics* **2011**, *203*, 18−21.

(49) Lightfoot, P.; Mehta, M. A.; Bruce, P. G. Crystal Structure of the Polymer Electrolyte Poly(ethylene oxide)$_3$:$LiCF_3SO_3$. *Science* **1993**, *262*, 883−885.


https://dx.doi.org/10.1021/acs.macromol.9b01725
*Macromolecules* XXXX, XXX, XXX−XXX

(50) Devanand, K.; Selser, J. C. Asymptotic behavior and long-range interactions in aqueous solutions of poly(ethylene oxide). *Macromolecules* **1991**, *24*, 5943−5947.
(51) Schünherr, H.; Frank, C. W. Ultrathin Films of Poly(ethylene oxides) on Oxidized Silicon. 2. In Situ Study of Crystallization and Melting by Hot Stage AFM. *Macromolecules* **2003**, *36*, 1199−1208.
(52) Carvalho, J. L.; Dalnoki-Veress, K. Homogeneous Bulk, Surface, and Edge Nucleation in Crystalline Nanodroplets. *Phys. Rev. Lett.* **2010**, *105*, 237801.
(53) Stolwijk, N. A.; Heddier, C.; Reschke, M.; Wiencierz, M.; Bokeloh, J.; Wilde, G. Salt-Concentration Dependence of the Glass Transition Temperature in PEO−NaI and PEO−LiTFSI Polymer Electrolytes. *Macromolecules* **2013**, *46*, 8580−8588.
(54) Zhang, X.; Yager, K. G.; Kang, S.; Fredin, N. J.; Akgun, B.; Satija, S.; Douglas, J. F.; Karim, A.; Jones, R. L. Solvent Retention in Thin Spin-Coated Polystyrene and Poly(methyl methacrylate) Homopolymer Films Studied By Neutron Reflectometry. *Macromolecules* **2010**, *43*, 1117−1123.
(55) Peng, Q.; Tseng, Y.-C.; Darling, S. B.; Elam, J. W. Nanoscopic Patterned Materials with Tunable Dimensions via Atomic Layer Deposition on Block Copolymers. *Adv. Mater.* **2010**, *22*, 5129−5133.


https://dx.doi.org/10.1021/acs.macromol.9b01725
*Macromolecules* XXXX, XXX, XXX−XXX